Towards Radiotherapy Enhancement and Real Time Tumor Radiation Dosimetry Through 3D Imaging of Gold Nanoparticles Using XFCT

Caroline Vienne[1(✉)], Adrien Stolidi[1], Hermine Lemaire[1], Daniel Maier[2], Diana Renaud[2], Romain Grall[3], Sylvie Chevillard[3], Emilie Brun[4], Cécile Sicard[4], and Olivier Limousin[2]

[1] CEA, LIST, DISC, 91191 Gif-sur-Yvette Cedex, France
caroline.vienne@cea.fr
[2] CEA/DRF/IRFU, CEA Saclay, 91191 Gif-sur-Yvette Cedex, France
[3] CEA/DRF/iRCM/LCE, CEA Fontenay, 92265 Fontenay-aux-Roses Cedex, France
[4] Université Paris Saclay, LCP, 91405 Orsay Cedex, France

Abstract. To enhance the efficiency of radiotherapy, a promising strategy consists in tumor exposure simultaneously to ionizing radiation (IR) and gold nanoparticles (GNPs). Indeed, when exposed to the radiation beam, these GNPs exhibit a photoelectric effect that generates reactive oxygen species (ROS) within the tumor and enhances the direct IR related deleterious effects. The measurement of this photoelectric effect thanks to an additional detector could give new insight for in vivo quantification and distribution of the GNPs in the tumor and more importantly for measuring the precise dose deposition. As a first step towards such a challenge, we present here materials and methods designed for detecting and measuring very low concentrations of GNPs in solution and for performing 3D reconstruction of small gold objects whose size is representative with respect to the considered application. A matrix image detector, whose sensitivity is first validated through the detection of few hundreds of micrograms of GNPs, is combined with a pinhole element and moved along a limited circular trajectory to acquire 2D fluorescence images of a motionless object. We implement a direct back-projection algorithm that provides a 3D image of these objects from this sparse set of data.

Keywords: X-ray fluorescence · Radiotherapy · Nanoparticles · CT

1 Introduction

The treatment of cancer is a major health challenge that mobilizes the scientific community from different fields. Due to the difficulty of eradicating resistant tumors, innovative approaches are proposed to enhance the efficiency of

A. F. Frangi et al. (Eds.): MICCAI 2018, LNCS 11070, pp. 401–409, 2018.
https://doi.org/10.1007/978-3-030-00928-1_46

radiotherapy. In the past decade, there has been a growing interest in using nanoparticles of high atomic number materials for dose enhancement and among them, gold nanoparticles (GNPs) offer several attractive features since they are generally considered chemically inert, biologically non-reactive and overall non toxic [1]. Depending on their size and on the route of administration, these nanoparticles can accumulate into the tumor, then during the radiotherapy, ionizing radiation (IR) will interact with the GNPs that will release free electrons. Once in contact with biological medium, those electrons will generate reactive oxygen species (ROS) and provoke an additional oxidative stress, compared to radiation alone, permitting to more effectively kill the tumor cells. In [2], Hainfeld et al. showed the beneficial effects of injecting GNPs to improve X-ray therapy. However, this promising idea faces a new challenge: up to now, there are no ways to know exactly how many GNPs reach the tumor and how long they are retained into it. All these data are crucial in order to estimate the applied radiative dose and to adjust GNPs delivery along the radiotherapy for optimizing the control of the tumor growth. To reach this goal, a promising idea consists in measuring the X-ray fluorescence of gold which follows the photoelectric effect [3,4]. By quantifying the intensity of Au-$K_{\alpha,\beta}$ fluorescence, it is possible to conclude on the concentration of GNPs in the tumor and on the IR dose. Fluorescence X-rays are commonly used for identifying the material composition of a given object but they can also be used when coupled with methods of tomography (XFCT), to determine the distribution of fluorescing elements. In this paper, we describe the considered setup based on the integration of a portable 16×16 pixels miniature imaging-spectrometer detector on a robotic arm. In Sect. 2, we present the materials and the performances of the proposed system for measuring GNPs in solution in view of biological aspects concerning the acceptable quantity of GNPs and dose that can be administered during radiotherapy. The second contribution of this paper concerns the validation of our XFCT strategy with this setup. A pinhole is added in front of the detector and the independent use of each pixel gives a 2D spectral image of a region of interest of a few centimeters. By moving the detector around this region of interest, a set of 2D images is acquired, post-processed and used as input of a back-projection algorithm for recovering the rough shape and dimension of small gold objects. XFCT results are detailed in Sect. 3. Due to the important drop of signal caused by the pinhole, the approach is here validated on pure gold objects but these first results pave the way for future optimizations.

2 Materials and Methods

An overall view of the proposed setup is displayed in Fig. 1. Both X-ray tube and detector are mounted on robotic arms, which facilitates the alignment of the setup and, above all, allows the acquisition of multiple views for XFCT approach. The detector is positioned at 90° of the X-ray beam in order to minimize the scattered radiation induced by ground.

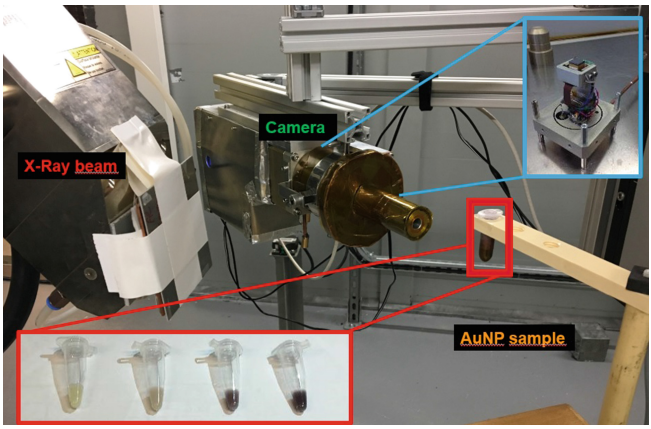

Fig. 1. View of the system. The X-ray beam is strongly filtered and collimated to create an incident pencil-beam with the desired spectral shape and the detector (camera) is also shielded by a collimator of 10 cm length and 1 cm diameter. In blue, the active surface of the detector without shielding is presented. In red, the different solutions of GNPs with increasing concentrations.

2.1 X-Ray Source Characteristics

A large majority of applications of XFCT are based on the use of a synchrotron source, which provides a bright monochromatic beam [5–7]. These beam characteristics are highly interesting for maximizing the efficiency of XFCT data acquisition since the incident energy can be selected according to the application. In particular, if a specific material is targeted, it is possible to choose the energy just above the absorption edge in order to obtain the best fluorescence signal. However, in practice, the use of synchrotrons is not realistic in laboratory or medical environments and polychromatic X-ray tubes have to be considered instead. The X-ray source used in this work is a Viscom XT 9225-D-ED microfocus tube used under 120 kV and at its maximum power (320 W). In order to limit the background noise during the measurement of the gold fluorescence, the X-ray tube is shielded with 1.4 mm of lead in addition to its native shielding and equipped with a 1 cm thick tungsten collimator, 3 mm in diameter. This collimator creates a circular illuminated region of 5 cm in diameter at the object position (30 cm from the source point).

2.2 Detector Performance and Calibration

The detector model is a CdTe imaging spectrometer namely Caliste-HD, which demonstrates high energy resolution over a large energy range [8]. This hybrid component is made of the assembly of one 16×16 pixel CdTe detector and eight analog front-end ASICs named IDeF-X HD equipped with 32 spectroscopic channels. Each pixel has a 625 µm pitch for a total size of the detector of 1 cm^2.

The main attractiveness to this design lies on the large energy range of the detector (1.5 keV to 1 MeV) and its good energy resolution down to 700 eV full width at half maximum (FWHM) at 60 keV. In the present configuration, the detector is installed into a light portable setup with limited cooling power. In addition to high count rates, the energy resolution degrades to 1.4 keV FWHM at 60 keV, still good enough for our demonstration. The energy resolution allows a good discrimination of the fluorescence X-rays lines for heavy metals such as gold. The whole detector chain is calibrated in energy thanks to a home-made plate covered with different element powders (Bismuth, Molybdenum, Tin, Gadolinium, Tungsten, Gold) that exhibit X-ray fluorescence lines at well-known energies. The plate is illuminated with the same X-ray source as used for the GNPs fluorescence.

When doing direct measurement of the fluorescence signal, the responses of the 256 pixels are summed up to generate the fluorescence spectrum. The performance of this detector for GNPs detection is validated using 1 mL of aqueous suspensions of GNPs at different concentrations. GNPs' size is 32 ± 6 nm. 20 min integration time is performed. The X-ray fluorescence of GNPs is clearly visible down to a mass of 144 µg of gold (see Fig. 2). A dose rate of 0.12 mGy/s at the location of the object is measured with a UNIDOS E dosemeter coupled with a TM 31013 PTW ionization chamber.

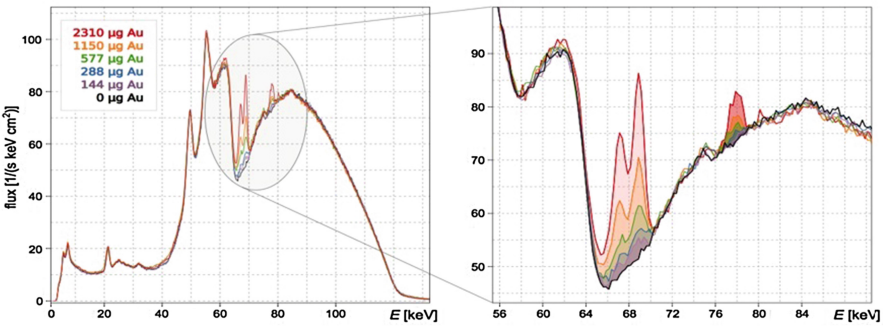

Fig. 2. Fluorescence spectrum obtained with different GNP concentrations in solution.

2.3 Pinhole X-Ray Fluorescence Imaging

For XFCT acquisition, a pinhole is added 10 cm in front of the image plane. This pinhole is made of 5 mm lead, attenuating all scattered or fluorescence signal, except for the aperture of 1 mm diameter. The distance between the pinhole and the object is 10 cm creating a magnification of 1 and allowing the inspection of a region of 1 cm^3. Contrarily to XFCT strategies based on a movable tightly collimated detector that inspects successively very small regions of the environment, the use of a pinhole coupled with a matrix image detector gives a direct 2D projection of the fluorescence distribution (see Fig. 3) and avoid additional

translational movements of the detector. Pinhole use has been investigated couples of years ago in another emission imaging such as SPECT and PET [9,10] and more recently by Jung et al. in a simulation study [11].

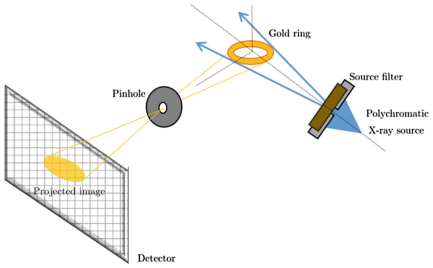

Fig. 3. Considered geometry for acquisition of XFCT data using a pinhole in front of the 2D detector.

3 XFCT Results

Due to the addition of the collimator and the use of the detector as an imaging spectrometer, which means that the signals from the 256 pixels are no longer summed up, the count of photons is greatly reduced in the XFCT configuration. For this reason, we chose here to validate the feasibility of our approach on pure gold objects with a representative size in a representative volume of interest (1 mm scale in a volume of few centimeters). Two small objects are considered in this case and described in Fig. 4.

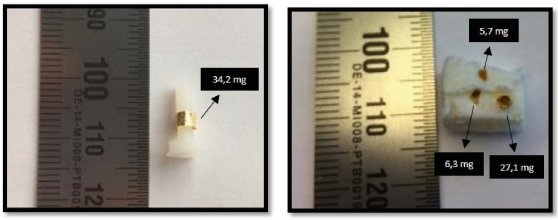

Fig. 4. Two gold samples used for XFCT: gold ring of 3 mm diameter and 1.2 mm height for 34.2 mg (left) and three pieces of gold of 1 to 2 mm size inserted in foam core with respective weight of 5.7 mg, 6.3 mg and 27.1 mg.

3.1 Acquisition Setup

The detector is now moved along a semi-circular trajectory around the sample in order to provide different views of the object. The acquisition plane crosses

the X-ray beam perpendicularly in order to ensure that the detector is always put at 90° from the X-ray incident beam and 26 images are acquired with an angular step of 10°, corresponding to a maximal angular range of 250° (see Fig. 5). This angular limitation in the trajectory aims at taking into account the limited accessibility around the human body during radiotherapy.

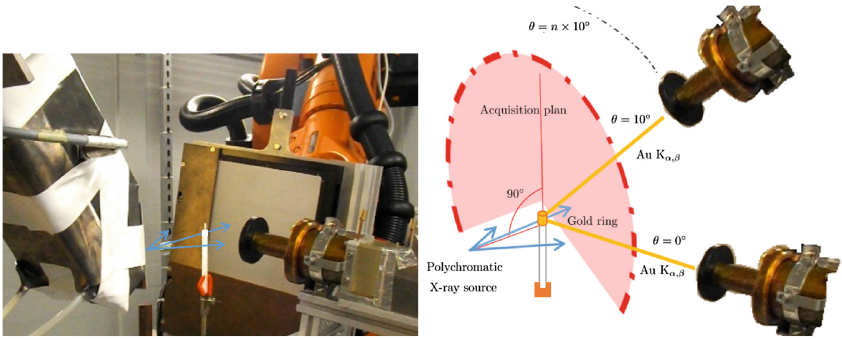

Fig. 5. Principle of XFCT data acquisition with the CdTe detector manipulated with the robotic arm.

3.2 Image Acquisition

For each pixel of the detector, the energy spectrum is recorded and 2D images are processed and used for the reconstruction. The 2D image of the gold ring corresponding to the first position of the detector along the trajectory ($\theta = 0°$) is displayed in Fig. 6. The left image corresponds to the complete spectrum. The second image corresponds to the hit-map of each pixel for all photons and the last one to the hit-map after selecting only photons whose energy is between 65 keV and 70 keV. Using the given spectrum, the energy resolution is about 1.9 keV FWHM at Au-K$_{\alpha_1}$.

Figure 7 shows three different fluorescence images of the ring object (first row) and of the three pieces of gold (second row) acquired for three different positions of the detector (−20°, 100°, 200°). The projection of the objects is clearly visible with pixels red to yellow (counts), the scattered homogeneous signal of the environment creates a dark blue background signal and the corners of the image, shielded by the collimator, have a zero value (black color). The acquisition time for each projection is 2 min, resulting in a total acquisition time of 52 min and a deposited dose of almost 400 mGy.

3.3 Image Reconstruction

A 3D reconstruction of both objects is performed from the 26 projections. Contrarily to classical tomographic imaging methods where the inversion of the

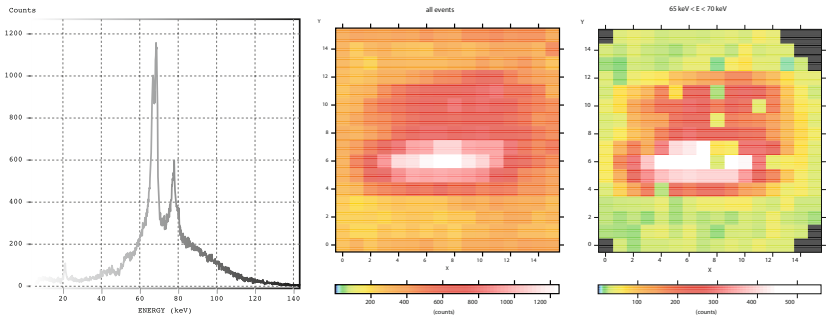

Fig. 6. Acquisition of a 2D image of gold fluorescence from the direct spectral signal measured in each pixel (left) to the corresponding hit-map created from all photons (center) and finally the hit-map for the photons whose energy is close to the energy range of the K_α fluorescence ray of gold ($\approx$ 68 keV)(right).

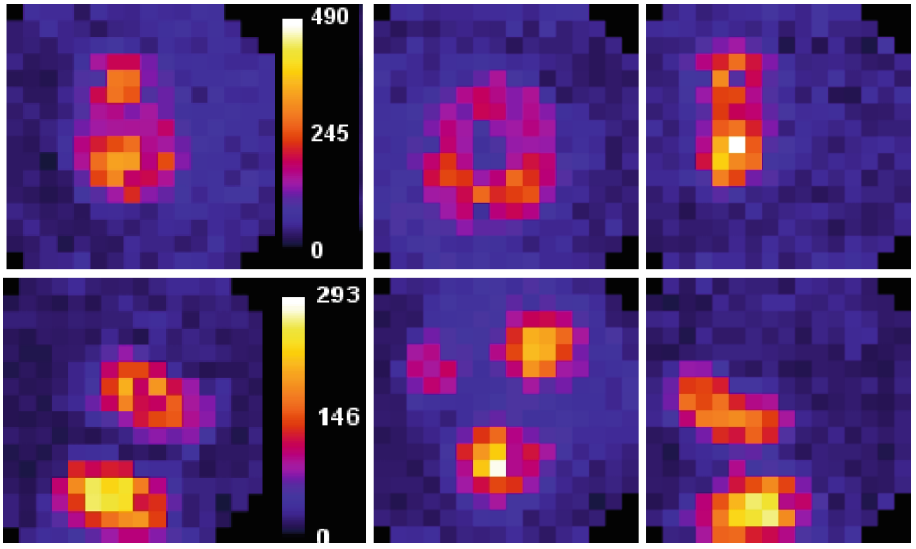

Fig. 7. Mutliple views of the gold objects provided by the 16 $\times$ 16 pixels detector.

Radon transform is based on Fourier back-projection methods, the reconstruction problem in XFCT involves iterative approaches that are better fitted for dealing with a sparse set of projections and a higher level of noise in the projections. Usually, maximum likelihood expectation maximization (MLEM) methods are chosen in this case. However, in our ideal conditions where the gold sample is put in an almost non attenuating foam, the object can be easily segmented from the background and we chose to apply a visual hull reconstruction approach [12] on the binarized images. The basic algorithm for visual hull extraction consists first in segmenting each input image in order to obtain the silhouette of the

object. Then, using the parameters of the acquisition system (pinhole-detector distance and pixel size), the silhouette from each image is projected to 3D space thereby creating a visual cone. Finally the visual hull is obtained as the intersection of all the visual cones generated for different points of view. Reconstruction results are presented in Fig. 8. The 3D space is discretized in $100 \times 100 \times 100$ voxels of size 100 µm. An isosurface is applied to the reconstructed volume to display the global shape and dimension of the objects and give a first visual validation of the approach. In addition, a cross section of the reconstructed volumes (b, d) is displayed for each object. The gold ring appears slightly deformed with a diameter of about 3.2 mm, close to real value of 3 mm and the three tiny objects are well separated, which confirms that the spatial resolution is better than 1 mm.

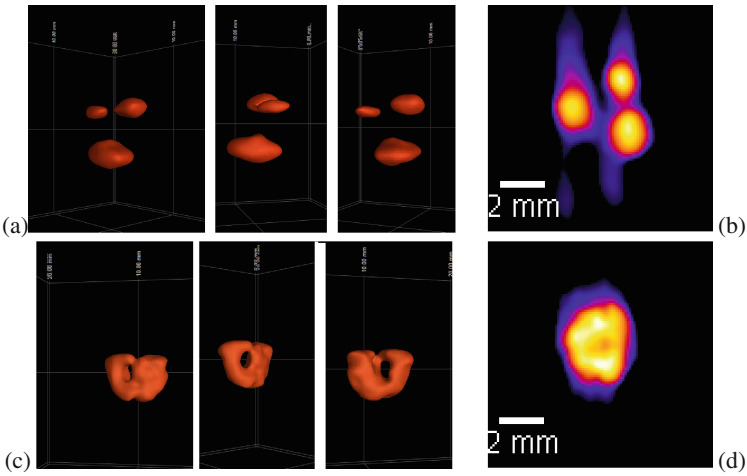

Fig. 8. Multiple views of the reconstructed objects (a, c) and cross section of the 3D images (b, d).

4 Conclusion

In this first step toward the validation of the feasability of measuring the dose deposited in the tumor during radiotherapy we focused on optimizing the system setup. A specific detector has been adapted and combined with a benchtop X-ray tube for this purpose. The sensitivity of the measurement has been validated on solutions with very low concentrations of GNPs. In addition, a first XFCT experiment has been successfully realized with small gold objects, representative in size of a tumor. The next two major steps of our developments consist in realizing XFCT of GNPs first in solution then in vivo.

References

1. Liu, A., Ye, B.: Application of gold nanoparticles in biomedical researches and diagnosis. Clin Lab. **8**(1–2), 23–36 (2013)
2. Hainfeld, J.F., Slatkin, D.N., Smilowitz, H.M.: The use of gold nanoparticles to enhance radiotherapy in mice. Phys. Med. Biol. **49**, 309–315 (2004)
3. Manohar, N., Reynoso, F.J., Diagaradjane, P., Krishnan, S., Cho, S.H.: Quantitative imaging of gold nanoparticle distribution in a tumor-bearing mouse using benchtop x-ray fluorescence computed tomography. Sci. Rep. **6**, 22079 (2016)
4. Le Loirec, C., Chambellan, D., Tisseur, D.: Image-guided treatment using an X-ray therapy unit and GNP: test of concept. Radiat. Prot. Dosim. **169**(1–4), 331–335 (2016)
5. Sunaguchi, N., Yuasa, T., Hyodo, K., Zeniya, T.: Fluorescent x-ray computed tomography using the pinhole effect for biomedical application. Opt. Commun. **297**, 210–214 (2013)
6. Sasaya, T., Sunaguchi, N., Lwin, T.T., Hyodo, K., Zeniya, T., Takeda, T., Yuasa, T.: Dual-energy fluorescent x-ray computed tomography system with a pinhole design: use of K-edge discontinuity for scatter correction. Sci. Rep. **7**, 44143 (2017)
7. Sasaya, T., Sunaguchi, N., Zeniya, T., Yuasa, T.: Multi-pinhole fluorescent x-ray computed tomography for molecular imaging. Sci. Rep. **7**, 5742 (2017)
8. Meuris A, et al.: Caliste HD: a new fine pitch Cd(Zn)Te imaging spectrometer from 2 keV up to 1 MeV. In: Nuclear Science Symposium Conference Record, pp. 4485–4488 (2011)
9. Jaszczak, R.J., et al.: Pinhole collimation for ultra-high-resolution, small-field-of-view SPECT. Phys. Med. Biol. **39**, 425–437 (1994)
10. Panin, V.Y., et al.: Fully 3-D PET reconstruction with system matrix derived from point source measurements. IEEE Trans. Med. Imaging **25**(7), 907–921 (2006)
11. Jung, S., Sung, W., Ye, S.J.: Pinhole X-ray fluorescence imaging of gadolinium and gold nanoparticles using polychromatic X-rays: a Monte Carlo study. Int. J. Nanomed. **12**, 5805–5817 (2017)
12. Laurentini, A.: The visual hull concept for silhouette based image understanding. IEEE Trans. Pattern Anal. Mach. Intell. **16**, 150–162 (1994)